Applied Thermal Engineering 64 (2014) 192–200

Contents lists available at ScienceDirect

Applied Thermal Engineering

journal homepage: www.elsevier.com/locate/apthermeng

Experimental analysis on frosting characteristic of SK-type finned refrigerating heat exchanger with large-diameter circular holes

Zhao-song Fang [a,b,c], Hou-hua Wang [a,b,c,*], Jie Zhang [d], Wei-wei Wu [a,b,c]

[a] Key Laboratory of the Three Gorges Reservoir Region's Eco-Environment, Ministry of Education, Chongqing University, Chongqing 400042, PR China
[b] Faculty of Urban Construction and Environmental Engineering, Chongqing University, Chongqing 400042, PR China
[c] National Centre for International Research of Low-carbon and Green Buildings, Chongqing University, 400045, PR China
[d] China Coal Technology & Engineering Group, Chongqing Design & Research Institute, Chongqing 400042, PR China

HIGHLIGHTS

- The large holes of SK-type induced the generation of turbulence flow.
- The refrigeration capacity and *COP* of SK-type exceeds that of plane one.
- The SK-type fin-and-tube heat exchanger is a new kind of heat transfer equipment.
- The defrost interval should not exceed 2 h under frost conditions.

ARTICLE INFO

Article history:
Received 20 June 2013
Accepted 14 December 2013
Available online 24 December 2013

Keywords:
SK-type fin
Heat transfer enhancement
Energy efficiency performance
Prototype frost test

ABSTRACT

This paper presents the construction of both a plane fin-and-tube heat exchanger and a SK-type fin-and-tube heat exchanger. Based on plane fin-and-tube heat exchanger, comparative industrial prototype experiments of SK-type fin-and-tube heat exchanger energy efficiency performance were carried out in the artificial climate chamber. Test results confirmed several findings: when the amount of the refrigerant charged is the same and face velocity $u = 3.75$ m s^{-1}, SK-type fin-and-tube heat exchanger refrigeration capacity increases by an average of 9.13%; energy consumption reduces by an average of 11.25%, coefficient of performance (*COP*) of heat exchanger increases by an average of 22.65% with continuous operation during the first 2 h. Also, when the operation time exceeds 2 h, the *COP* of both types of heat exchangers are both less than 0.6, illustrating that under frost conditions, the defrost interval should not be too long, otherwise energy consumption may sharply spike.

1. Introduction

In traditional heat exchangers, the rectangular plane fin has marked advantages over competing designs, such as a simple structure that is easy to clean and process, strong adaptability, etc. Accordingly, it is widely used in various industries including power, chemical, petroleum, aerospace, air conditioning and refrigeration. However, under dry and wet conditions, heat transfer performance of the rectangular plane fin is poor, and subsequently in these areas it has been replaced by more efficient designs such as the corrugated fin, slit fin or louver fin [1]. Each of these designs also suffers from performance issues—frost accumulation on the surface of the fin during heat transfer leads to the aperture of those "efficient fins" becoming easily clogged by the frost layer, leading to a loss of heat transfer capability enhancement, and making the exchanger itself less effective.

The shortcomings of the existing fin designs along with the growing need for high efficiency heat exchangers and their significance for energy conservation make the development of a new fin with high efficiency heat exchange under frost conditions critical. Previous studies on the performance of the fin-and-tube heat exchanger under frost condition mainly focused on two aspects. The first was modeling the fin surface frost layer increase [2–6], which includes one of the most notable previous studies by Lee [5]. In 2006, he developed a mathematical model to predict the thermal performance of a fin-tube heat exchanger under frosting conditions. The second focus was on the heat transfer effect of different

* Corresponding author. Faculty of Urban Construction and Environmental Engineering, Chongqing University, Chongqing 400045, PR China. Tel.: +86 23 65121647.
E-mail address: whhxinxiang@aliyun.com (H.-h. Wang).

1359-4311/$ – see front matter Crown Copyright © 2013 Published by Elsevier Ltd. All rights reserved.
http://dx.doi.org/10.1016/j.applthermaleng.2013.12.030

forms of the heat exchanger fins on the air side [7–11]. Generally, refrigeration heat transfer performance of louver fin was fond to be superior to that of the plane fin under dry and wet conditions, so it is widely used in air-conditioning. However, under frost conditions, both fins are easily covered by the frost lay and lose their heat transfer enhancement. To date, studies on heat transfer enhancement of new fin heat exchangers are quite rare.

Recently, Hou-hua Wang et al., [12] designed three types of geometry deformable sheets of rectangular plane fin to conduct some experiments that compare it with the rectangular plane fin. The results showed that the average equivalent surface heat transfer coefficient of circular holes fin was 13.4% higher than the plane fin tube. Based on this study, Hua Su [13] later developed a type of plane fin with holes on both sides and conducted some orthogonal experiments, which showed that when under dry conditions, the surface heat transfer coefficient of an optimized dual symmetrical circular holes fin was 14.55% higher than plane fin, while also saving materials up to 10%.

Jian-wei Gao [14,15] carried out comparative experiments on the refrigeration performance of circular-semi hole crossed fin, double circular holes fin, and plane fin tubular heat exchangers under frost conditions by utilizing the refrigeration system of the refrigerator. The results proved that double circular holes fin-and-tube heat exchanger had a better refrigeration effect alongside a 3.9% power savings under the same refrigeration capacity. Throughout the experiment, due to the fin's large diameter holes, the overall heat transfer enhancement performance was still maintained though a small amount of circular holes were blocked by the frosting layer.

Zhao-song Fang [16] studied the characteristics of flow and heat transfer via numerical simulation, and analyzed the weak heat transfer local position of the fin heat exchanger surface, creating a theoretical basis for the position of large diameter circular holes. Based on this study, a type of patent fin with three symmetrical circular holes in fin [17] known as a SK-type circular holes fin was used as shown in Fig. 1(1). The SK-type fin has several distinguishing features: in each fin, along the direction of airflow, two holes with diameter D are opened symmetrically front and back of basic tube by pivoting the center of base tube. The half-circular hole spacing is e and the center distance is l. In each fin, perpendicular to the direction of airflow, a hole with diameter D is opened at each $Y/2$ of the two basic tube axial centers. The width of the fin is W. The outer diameter of the basic tube is D_0, and the spacing of basic tube is Y. The followings are the relative relationship between the various geometry sizes: $D/D_0 = 0.48–0.58$, $l/D_0 = 0.84–0.88$, $e/D_0 = 0.50–0.54$, $Y/D_0 = 2.9–3.2$, $W/D_0 = 2.4–3.4$.

Choosing rectangular plane fin as comparative subject, Hou-hua Wang and Zhao-song Fang [18] analyzed flow and heat transfer characteristics on the same dimensions of a SK-type fin-and-tube heat exchanger via numerical simulations. The results showed that as compared with the plane fin, the surface heat transfer coefficient of SK-type fin increases by 25.7% on average during the same range of velocity. Essentially, the SK-type fin's effect of heat transfer enhancement was excellent. Comparing simulation results with available experimental data, the relative error between them was below 10%, validating the conclusions of the numerical simulations. Meanwhile, Hou-hua Wang et al. [19], also conducted a study on the energy conservation performance of a refrigeration heat exchanger with single row of fin tubes under frost conditions in wind tunnel instrumentation. The result showed that when the average face velocity was between 1.87–5.00 m s^{-1}, the refrigeration capacity of the SK-type fin-and-tube heat exchanger increased by 3.0%–16.8%, with an average increase of 9.0% over the plane fin-and-tube heat exchanger. The surface heat transfer coefficient likewise increased by 49.7%–80.1%, with an average increase of 64.3%. The coefficient of performance (*COP*) increased by 15.0%–30.2%, with an average increase of 23.0%. The resistance was also reduced by an average of 32.0%. Over the course of 5.5 h under frost conditions, only some circular holes are blocked by the frost layer on the surface of SK-type fin-and-tube heat exchanger, but the exchanger still maintained the excellent characteristics of heat transfer enhancement.

Numerical simulations and experimental studies under frost conditions together confirmed that the SK-type large diameter circular holes fin is in fact an excellent design, suitable for a refrigeration heat exchanger. This design possesses better performance of heat transfer and resistance than the traditional rectangular plane fin under frost conditions, and does so with remarkable energy conservation. Moreover, because of the large diameter of the holes, they could not be as easily be blocked by the frost layer. This design also maintains the excellent characteristics of heat transfer enhancement during defrost intervals. Therefore, the SK-type large diameter circular holes fin is a viable alternative of the currently used plane fin-and-tube heat exchanger. To move forward and accelerate the development of new product and push it into the market, it is necessary to verify the correctness of the laboratory test results. To that end, in this paper the authors conducted a

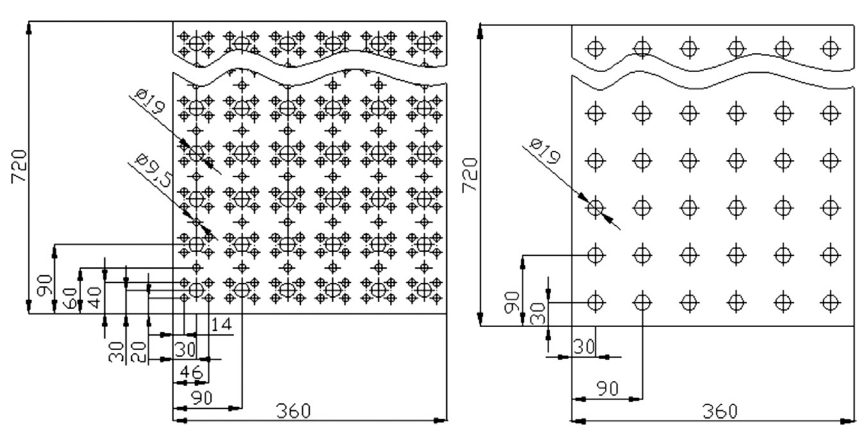

(1) (2)

Fig. 1. Fin structure of (1) the SK-type and (2) the plane fins.

comparative study on a prototype SK-type fin-and-tube refrigeration heat exchanger and compared its performance with that of a plane fin-and-tube heat exchanger in a climate chamber.

2. Experimental setup

2.1. Fin structure

In this paper, two types of fin-and-tube refrigeration heat exchanger prototypes, the SK-type fin-and-tube refrigeration heat exchanger and the plane fin-and-tube refrigeration heat exchanger are investigated. Each fin consists of six rows of tubes that are of a fast-refrigeration type. The basic dimensions of the fins are as follows: the basic tube diameter D_0 is 19 mm, fin thickness δ is 0.5 mm, tube spacing Y is 60 mm, fin spacing S is 10 mm, fin width W is 360 mm, and length C is 720 mm. There are no holes on the surface of rectangular plane fin. In the SK-type fin, two symmetrical holes are opened on the front and back of the basic tube, and a hole is opened at the center of the two basic tubes. Hole spacing e is 20 mm; center distance between holes and basic tube l is 14 mm, as shown in the design of the SK-type fin in Fig. 1(1). Plane fin structure dimensions are shown above in Fig. 1(2). Prototypes are composed of an aluminum jacket and galvanized steel shell with external dimensions of 1400 × 850 × 1000 mm, as shown in Fig. 2.

2.2. The test system

The test was conducted in artificial climate chamber at the Laboratory Center of School of Urban Construction and Environmental Engineering, Chongqing University. The chamber is 7 m × 6 m × 3 m without windows and with only one thermal insulation door. The wall structure is: Insulation structure from the outside-to-inside of interior wall and the ceiling's structural layer is 3 mm thickness of colored steel plate (coefficient of thermal conductivity was 0.027 W $(mk)^{-1}$), 100 mm thickness of polyurethane foaming agent (coefficient of thermal conductivity was 0.035 W $(mk)^{-1}$), and 3 mm thickness of stainless steel surface; insulation structure of the floor from bottom to top is: a structural layer of 3 mm thickness of linoleum, 100 mm thickness of polystyrene layer (coefficient of thermal conductivity was 0.03 W $(mk)^{-1}$), and 20 mm thickness of terrazzo floor. To control the environment of chamber, constant temperature and humidity equipment was installed that are capable of keeping the temperature below 0 °C. The construction insulation of the artificial climate

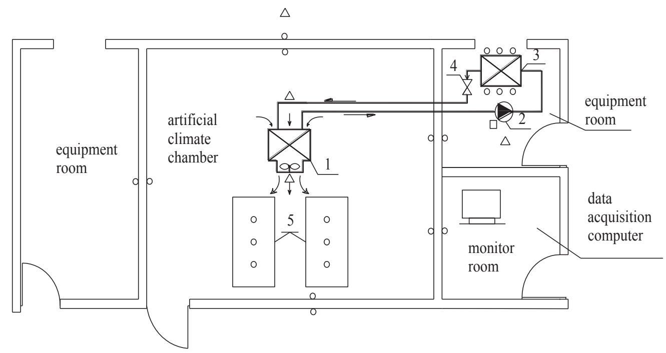

Fig. 3. Experimental principle and the measuring point plan.

chamber was strictly conducted according to relevant standards of refrigeration storage, with an excellent insulation effect. Initial test results affirm that the heat loss through the envelop are negligible. In this paper, the experiment system consisted of a refrigeration system and a measuring system, as shown in Fig. 3.

The two kinds of fin-and-tube heat exchangers prototypes were installed in the artificial climate chamber. The compressor and condenser were installed in the equipment room. The refrigeration system consisted of an evaporator, compressor, condenser and thermal expansion valve. When the system was running, refrigerant went through the condenser and the thermal expansion valve before moving into the prototype (evaporator). During the refrigeration cycle, the refrigerant absorbed heat to become a gaseous refrigerant in the evaporator and was then absorbed by the compressor, finishing the refrigeration cycle. In the air side, indoor air was forced to circulate through the prototype to be refrigerated. In order to make accurate measurements of the refrigeration capacity of the prototype, two water tanks of 1.8 cubic meters were placed to absorb the refrigeration capacity in the chamber.

In Fig. 3, temperature measuring point symbol “” was used for measuring air temperature, water temperature and wall surface temperature, which were automatically recorded by the thermocouple connecting the apparatus to the data acquisition instrument. The temperature and humidity measuring point symbol “△” was used for measuring air temperature and humidity, which were automatically recorded by a Tinytag Ultra 2 data recorder. Measuring point layout positions are shown in Fig. 3. Inlet and outlet air temperatures of the condenser were measured by three

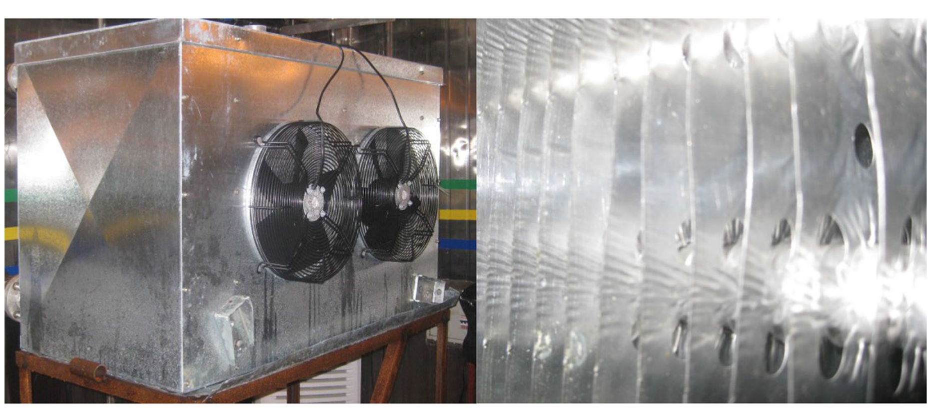

(1) (2)

Fig. 2. Photos of (1) SK-type prototype shape and (2) of partial fins of SK-type prototype. 1. Prototype, 2. compressor, 3. condenser, 4. expansion valve, 5. tank; . temperature measuring point; △ dry bulb temperature and relative humidity measuring point, □. power consumption measuring point.

Table 1
Accuracy and range of instrumentation used in the experiment.

Measured parameter	Instrument	Accuracy	Range
Temperature	T-type thermocouple	±0.15 °C	−50 °C to +500 °C
Air dry temperature and relatively humidity	Tinytag Ultra 2 data recorder	0.3 °C; ±3%RH	−25 °C to +85 °C; 0–95%RH
Power consumption	Multifunction power meter-B600Y	±1%	0–100 kW h

pairs of thermocouples with a uniform arrangement. The inside and outside wall surface temperature of artificial climate room was measured by five pairs of thermocouples. The tank size was 3 m × 1 m × 0.6 m. During the experiment, water in the tanks had a depth of 0.2 m. In order to consider the water temperature stratification, three pairs of thermocouples were uniformly set at each location of measuring points along the depth direction of the water, so that each tank had 6 pairs of thermocouples in total. The compressor power consumption was measured by an electricity meter, denoted by the symbol "□". Indoor and outdoor air wet bulb temperatures were measured at 4 measuring points and automatically recorded by a Tinytag Ultra 2 data recorder. All measuring instruments were strictly checked and tested to ensure they were in line within the manufacturer's specifications and met the demand of this experiment. The accuracy, range of the instrumentation is summarized in Table 1.

2.3. Experimental procedure

R22 was used as refrigerant for the experiment and the amount of filling R22 was controlled strictly according to the weight method. The amount of refrigerant used to test the SK-type fin prototype and plane fin prototype was completely equal. Experimental steps were as follows:

(1) The constant temperature and relative humidity equipment was operated until indoor air temperature and relative humidity met the baseline requirements;
(2) The fan in front of compressor and evaporator was operated 10 min after the measuring system began to measure;
(3) Parameters were recorded every 10 min, and measurements were directly inputted into a computer, using an Excel spreadsheet for data storage and analysis. The experiment process lasted 4 h. Face wind velocity was 3.75 m s^{-1} at the beginning of the experiment.

To obtain comparable results, indoor and outdoor air conditions over the course of 12 days were analyzed, and two groups of experimental data were used which detailed information have been shown in Table 2. It should be noted that the difference in outdoor dry bulb temperatures only influences heat transfer of the envelope. Heat loss through the envelope, however, was less than 0.6% of refrigeration capacity, and accordingly had little impact on accurately calculating the prototype refrigeration capacity.

3. Data processing method

Experimental data was processed according to the following formula:

(1) Refrigeration capacity Φ_0

According to the measured data, the average refrigeration capacity of heat exchanger was calculated in 10 min period using Equation (1) as follows:

$$\Phi_0 = \Phi_s + \Phi_e + \Phi_a + \Phi_w + \Phi_k \tag{1}$$

where

Φ_s—the average refrigeration capacity of water absorbed due to temperature decreasing during 10 min period, W;
Φ_e—the average refrigeration capacity of the equipment absorbed in artificial climate chamber during 10 min period, W;
Φ_a—the average refrigeration capacity of the air absorbed in artificial climate chamber during 10 min period, W;
Φ_w—the average refrigeration capacity of the envelope absorbed during 10 min period, W;
Φ_k—the average refrigeration capacity caused by the envelope heat loss during 10 min period, W.

(2) The refrigeration capacity of water absorbed Φ_s

Each of the two tanks had 6 thermocouples placed on them to measure changes in temperature. Accordingly, the average of the six measured values was calculated using Equation (2), to give the average refrigeration capacity of water absorbed:

$$\Phi_s = \frac{m_s c_p \Delta t}{10 \times 60} \tag{2}$$

where

m_s—the water mass quantity in the tank, kg;
c_p—the water constant-pressure specific heat of the average temperature during measurement period, J (kg K)$^{-1}$;
Δt—the average temperature difference between the first two measurements, °C.

(3) The refrigeration capacity of equipment absorbed Φ_e

There were two refrigeration chillers and two steel tanks whose qualities were all known in an artificial climate chamber. Therefore, the average refrigeration capacity of equipment absorbed Φ_e including the refrigerating capacity of the absorbed refrigeration chillers and steel tanks were calculated according to Equation (3):

$$\Phi_e = \frac{m_{e1} c_{e1} \Delta t_1 + m_{e2} c_{e2} \Delta t_2}{10 \times 60} \tag{3}$$

where

m_{e1}—cooled chiller mass quantity, kg;
m_{e2}—steel tank mass quantity, kg;

Table 2
Comparison of indoor and outdoor dry bulb temperature and relative humidity.

Working condition	Fin type	Outdoor dry bulb temperature	Outdoor relative humidity	Indoor dry bulb temperature	Indoor relative humidity
Case1	Plane fin	37.1 °C	60%	30.2 °C	66%
	SK fin	39.1 °C	57%	30 °C	64.1%
Case2	Plane fin	33.2 °C	62.9%	29.6 °C	69%
	SK fin	33.1 °C	72%	29.9 °C	71.7%

c_{e1}—constant-pressure specific heat of cooled chiller, J (kg K)$^{-1}$;
c_{e2}—constant-pressure specific heat of steel tank, J (kg K)$^{-1}$;
Δt_1—the temperature difference between the first two measurements of refrigeration chiller, °C;
Δt_2—the temperature difference between the first two measurements of steel tank, °C.

Among them, the chiller body temperature was measured by a thermocouple embedded in the chiller body.

(4) The average refrigeration capacity of air absorbed in artificial climate chamber Φ_a

$$\Phi_a = \frac{\rho_a V(h_{a,k} - h_{a,k+1})}{10 \times 60} \tag{4}$$

where

ρ_a—the air density of average temperature in the measurement period, kg m^{-3};
V—the volume of artificial climate chamber m^3;
$h_{a,k}$, $h_{a,k+1}$—mass quantity enthalpy of first two measurements of moist air in the artificial climate chamber, J kg^{-1};
k—number of measurement points in chronological order.

Mass quantity enthalpy was obtained by the indirect method, through the aforementioned Tinytag data recorder that measures the dry bulb temperature and relative humidity of wet air, and checks the enthalpy humidity chart to derive the mass quantity enthalpy.

(5) The refrigeration capacity of envelope absorbed Φ_w

The artificial climate chamber envelope structure included one external wall, three internal walls, one ceiling and a floor. Its thermal insulation structure in the front had been described in detail. Except for the floor, the rest of the envelope surface was composed of a surface layer of 3 mm thick stainless steel plate. The average refrigeration capacity of the envelope absorbed Φ_w was calculated as the sum of refrigeration capacity of layers material absorbed according to Equation (5):

$$Q_w = \sum_{i=1}^{m} \rho_i \delta_i A_{w,i} c_i \Delta t_i \tag{5}$$

where

ρ_i—the density of the i-layer material, kg m^{-3};
δ_i—thickness of the i-layer material, m;
$A_{w,i}$—the surface area of the i-layer material, m^2;
c_i—the specific heat capacity of the i-layer material, J (kg K)$^{-1}$;
Δt_i—the average temperature difference between the two measurements of the two surfaces of the i-layer material during the 10 min, in °C. Δt_i was calculated according to Equation (6):

$$\Delta t_i = \left(\frac{t_i^k + t_{i+1}^k}{2} - \frac{t_i^{k+1} + t_{i+1}^{k+1}}{2}\right) \tag{6}$$

where

i denotes the material layer number, $i = 1$ means the inner surface, $i = 2$ means the interface of the first and the second layer of material;
k denotes the time sequence number of temperature measuring point, $k = 1$ means the first measurement, $k + 1$ means the second measurement after 10 min of the k-th measurement.

(6) The heat transfer capacity of envelope Φ_k

$$\Phi_k = \sum_{j=1}^{6} k_j A_{w,j} \Delta t_j \tag{7}$$

where the j-th heat transfer coefficient of the wall is as follows:

$$k_j = \frac{1}{\sum_{i=1}^{n} \frac{\delta_i}{\lambda_i}} \tag{8}$$

In formulas (7) and (8):

$A_{w,j}$—the heat transfer area of j-th wall, m^2;
Δt_j—the average temperature difference of heat transfer of the j-th wall, taking the average measured temperature of first two measurements of outer and inner surfaces, *Co*;
δ_i—the thickness of the i-layer material, m;
λ_i—the thermal conductivity of the i-th layer material, W m^{-2} °C^{-1};
n—the material layers' number.

Materials of wall: structural layers (thermal conductivity was 0.54 W (mK)$^{-1}$, thickness was 240 mm); Color steel plate (thermal conductivity was 0.027 W (mK)$^{-1}$, thickness was 3 mm); polyurethane foam (thermal conductivity was 0.035 W (mK)$^{-1}$, thickness was 10 cm); stainless steel (thermal conductivity was 48.5 W (mK)$^{-1}$, thickness was 3 mm).

(7) The heat release capacity of the air Φ_1

The wet air's state changed after flowing through the heat exchanger. The status of the wet air in-and-out of the heat exchanger were measured by Tinytag Ultra 2 data recorders, and then the heat release capacity of the air was calculated by the enthalpy difference method as in Equation (9).

$$\Phi_1 = \dot{m}_a (h_{a,i} - h_{a,0}) \tag{9}$$

where

$\dot{m}_a$—mass flow rate of wet air, kg s^{-1};
$h_{a,i}$, $h_{a,0}$—wet air enthalpy mass quantity of inlet and outlet, J kg^{-1}, taking the average of the first two measurements.

(8) The heat release capacity of the condenser Φ_2

In the condenser, the release heat capacity of per unit time should be equal to the heat absorption capacity of evaporator plus the power consumption of the compressor. Without consideration of heat loss, the part of the heat flow rate should be equal to the air heat absorption. So, heat absorption capacity per unit time of cooling air was calculated according to Equation (10):

$$\Phi_2 = \dot{m}_{a2} c_{pa} (t_{a,0} - t_{a,i}) \tag{10}$$

where

$\dot{m}_{a2}$—the air mass flow through the condenser, kg s^{-1};
c_{pa}—the specific heat capacity at constant pressure of air, J (kg °C)$^{-1}$;

$t_{a,0}$,$t_{a,i}$—the air temperature that goes through the condenser outlet and inlet respectively, °C, was measured by the thermocouple.

In this experiment, the heat balance error was to be met by calculating Equations (11) and (12):

$$\Delta_1 = \left|\frac{\Phi_0 - \Phi_1}{\Phi_0}\right| \times 100\% \leq 5\% \tag{11}$$

$$\Delta_2 = \left|\frac{\Phi_0 + P - \Phi_2}{\Phi_0 + P}\right| \times 100\% \leq 5\% \tag{12}$$

(9) Coefficient of performance (*COP*) of compressor

The definition of *COP* of compressor is:

$$COP = \frac{\Phi_0}{P} \tag{13}$$

where P is the power consumption of compressor per unit time, W, which is measured by power meter, kW h. Measurement time is 10 min. Therefore, *COP* was calculated according to Equation (14):

$$COP = \frac{600\Phi_0}{3.6 \times 10^6 P} = \frac{\Phi_0}{6 \times 10^3 P} \tag{14}$$

where the unit of P is kWh.

4. Results and discussion

4.1. Comparison of the refrigerating capacity

Calculations by Formula (1), changes in the refrigeration capacity of heat exchangers with time in the process of operation are shown in Fig. 4, showing the change under condition 1 and condition 2. In Fig. 4, it is worth noting a few points: the horizontal time axis corresponds to the refrigeration capacity of the heat exchanger, and the horizontal line above corresponds to the percentage of hourly refrigeration capacity to maximum refrigeration capacity. In Fig. 4, at the beginning of operation, the refrigeration capacity increases with the change of time, and then decreases. In this study, the different cooling effects of both the SK-type and Plane fin heat exchangers were investigated. As such, the sampling frequency at the beginning of the experiment was not been fractionized. Based on the experiment, the highest refrigeration capacity should occur around 20 min, leading to an efficient operation time at 30 min in front of operation. The main reason for this timing is that when the evaporator begins to refrigerate, the surface temperature is lower than the dew point temperature of the air and also below 0 °C, so that discontinuous frost crystals begin to appear on the surface of the fins [16,19]. At that time, the rough frost grains on the surface not only expand the heat transfer area of the finned tube, but also enhance the airflow disturbance, which increases the refrigeration capacity. However, as the time increases, the area of the frost layer increases, covering the fin surface and increasing the thermal insulation, thereby reducing the area of air flow, and accordingly the refrigeration capacity also decreases concurrently [6]. The refrigeration capacities of the two conditions clearly illustrate the same change rule, that can be seen from the curve in refrigeration capacity that occurs when the heat exchanger runs for 2 h and the refrigeration capacity declines sharply from the maximum of around 19000 W to less than 4000 W. At that time, the refrigeration capacity is only about 20% of the maximum. With the increase of operation time, the refrigeration capacity continues to decline, but does so more slowly because the growing thermal insulation of the frost layer is large, seriously affecting the heat transfer effect between the air and the evaporator, thus necessitating the system to stop running to defrost.

As clearly shown in Fig. 4, the refrigeration capacity of the SK-type fin-and-tube evaporator is noticeably larger than that of the plane fin-and-tube evaporator: the highest refrigeration capacities of the plane fin and the SK-type fin are 19041.85 W and 19474.98 W, respectively, under condition 1, and 18112.77 W and 21285.24 W, respectively, under condition 2. On average then, the SK-type is higher by 1802 W. The results of the analysis outlined in Fig. 4 and the refrigeration capacity of the evaporator within 2 h are shown in Table 3. Since the holes on the SK-type fin surface create a good turbulence effect for incoming flow and effectively destroy the flow boundary layer, the heat transfer is enhanced at the air side [18]. While the refrigeration capacity is notably larger in the SK-fin than the plane fin, as the running time increases, the area becomes covered by the frosting layer increases and the refrigeration capacity decreases. During this cycle, the circular holes on the SK-type fin are not completely covered, allowing them it to have an effect of

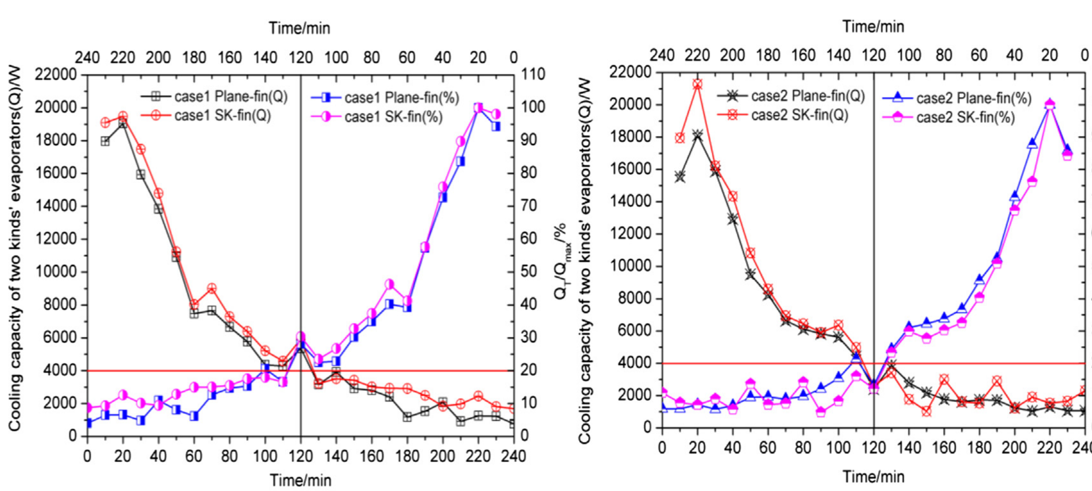

(1) (2)

Fig. 4. Refrigerating capacity and percentage changes over time of (1) Working condition 1 and (2) Working condition 2.

Table 3
Comparison of refrigerating capacities between two types of finned tube-type cooling heat exchangers.

Time (min)	Case 1			Case 2		
	Refrigerating capacity of SK-type prototype (W)	Refrigerating capacity of plane fin prototype (W)	Increase of SK-type over plane prototype (%)	Refrigerating capacity of SK-type prototype (W)	Refrigerating capacity of plane fin prototype (W)	Increase of SK-type over plane prototype (%)
10	19095.459	17960.03	6.32%	17948.42	15549.51	15.43%
20	19474.981	19041.85	2.27%	21285.24	18112.77	17.52%
30	17482.765	15935.99	9.70%	16217.46	15887.81	2.08%
40	14789.642	13840.61	6.85%	14324.21	12927.34	10.81%
50	11236.486	10917.82	2.91%	10831.69	9497.778	14.05%
60	8035.283	7483.722	7.37%	8590.284	8252.058	4.10%
70	9010.3996	7661.973	17.60%	6935.857	6644.891	4.38%
80	7289.9502	6666.661	9.35%	6449.16	6122.313	5.34%
90	6387.7018	5769.423	10.70%	5905.975	5837.677	1.16%
100	5215.3783	4349.464	19.90%	6365.386	5622.882	13.22%
110	4590.5117	4292.571	6.94%	4982.079	4406.674	13.07%
120	5926.887	5366.741	10.44%	2588.052	2406.022	7.56%

Average increase of SK-type fin over plane fin: Case 1 (9.20%); Case 2 (9.06%); Total (9.13%).

heat transfer enhancement. On the whole, within the running time of 2 h, the refrigeration capacity of SK-type finned evaporator is significantly larger than plane fin-and-tube evaporator, increasing by 9.13% on average, meaning that the SK-type fin has a comparatively stronger heat transfer enhancement in subzero refrigeration.

Real photos of frosting on the finned surface while SK-type prototype is running at 20 min, 60 min, 90 min and 120 min which are shown in Fig. 5. The photos show that on the whole, there is only a small quantity of frosting grains on the fin surface. As time increases, frosting grains increase on the fin surface and broaden the area of heat exchange and thus enhance the overall disturbance. On the whole, this is advantageous for heat exchange, and the experimental results show that heat exchange effect is optimized at that time. As time goes on further, the frosting layer incrassates along the surface of the basic tube to the radial direction, at the same time, the frosting thickness on the surface of the basic tube is significantly greater than that on the surface of the fin for several reasons: (1) Refrigerant enters into the heat exchanger from the bottom drains and out from the top, as the basic tube at the bottom is connected to the throttle valve, and accordingly the temperature difference between the air-side and refrigerant-side is larger at bottom basic tube than at the top basic tube [20]; (2) Due to gravity, the condensed water flows down from the top of the fin, and pools at the bottom; and (3) The temperature of the surface of the basic tube is lower, which rapidly cools the air sweeping the basic tube, and the water vapor in the air rapidly precipitates to form a frost, as shown in Fig. 5(2). The result noted in this experiment is similar as that found in Lee's study [20]. Once the compressor has run for 90 min (Fig. 5(3)), the fin surface is covered by a frosting layer, the air flow passage in the middle of the basic tube is congested, and the frosting layer on the fins does not appear to link together to form a solid sheet momentarily. When the compressor had run for 120 min (Fig. 5(4)), the frosting layer on the fins incrassates noticeably, and the thickness of the frosting layer at the bottom is at its maximum. The localized frosting layer on the respective fins near the basic tube link together, and the air flow passage in the middle of the substrate tube is completely blocked. At this point, the incoming flow of the fan decreases significantly, the side face begins to flow, the refrigeration capacity decreases, and defrosting becomes necessary.

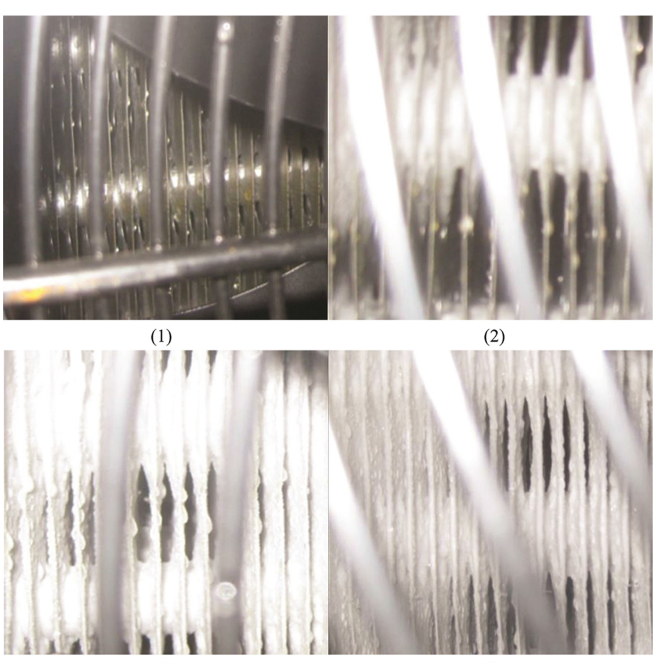

Fig. 5. Frosting condition on the finned surface at different running times of (1) running for 20 min, (2) running for 1 h, (3) running for 1.5 h and (4) running for 2 h.

4.2. Comparison of power consumption

Fig. 6 illustrates the variance in power consumption of the two heat exchangers as running time goes on in different conditions. Power consumption of the compressor seems to decrease continuously with the growth of the running time, particularly within the first 2 h. After the running time has gone on beyond 2 h, power consumption becomes relatively stable and changes little. This stable state is primarily due to fact that after the evaporator has been running for a certain time, the whole surface becomes covered by the frosting layer, leading to a decline in refrigeration capacity, which becomes relatively small but stable. Comparing the two heat exchangers, the power consumption of the plane fin-and-tube heat exchanger is significantly larger than SK-type fin heat exchanger (11.25% higher on average after the first 2 h). The power consumption of the SK-type fin heat exchanger is so much lower because the heat transfer efficiency of the cooling heat exchanger are improved concurrently in the SK-type fin, allowing the low-pressure liquid flowing into the evaporator to be transformed into low-pressure gas more effectively. The liquid refrigerant content in the refrigerant flowing out from the SK-type fin-and-tube

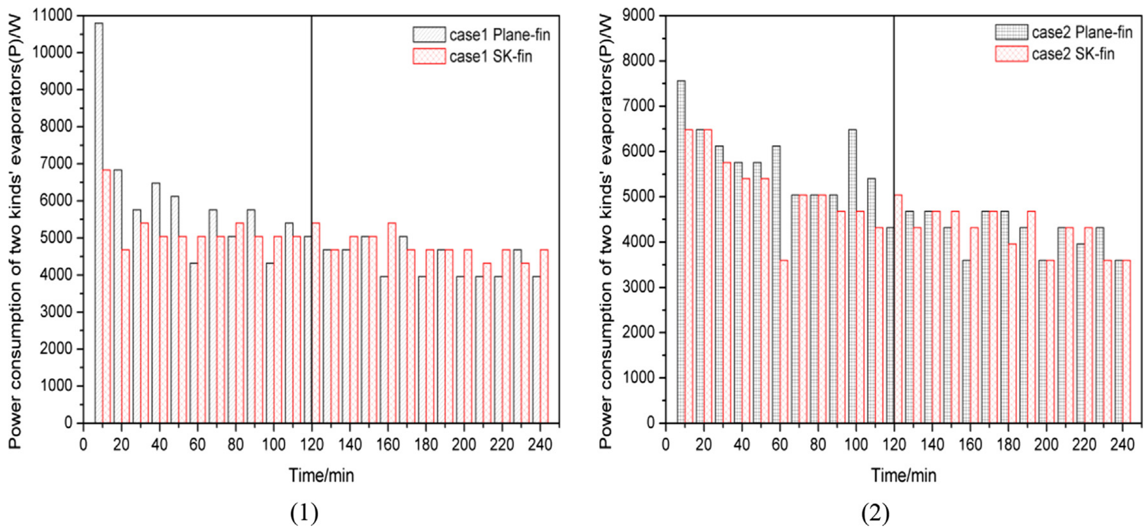

Fig. 6. Power consumption over the course of 4 h running time of (1) Working condition 1 and (2) Working condition 2.

heat exchanger is then less than that found in the plane fin heat exchanger, consuming less energy when re-entering the compressor cycle.

4.3. The comparison of COP

COP is the main technological and economic index to measure energy consumption of the refrigerator. Fig. 7 illustrates the changing curve of *COP* along with the running time at 2 h under working conditions. The curve showed that for the two types of heat exchangers, the *COP* has a different increase in amplitude with the frosting grains gradually forming at the beginning of the operation. However, with as the operation time grows, the frosting grains couple together to form a frosting layer that gradually incrassates, thus explaining the decreases in *COP*. After a running time of 120 min, the *COP* value is below 0.6, meaning that the main technological and economic indexes of the two types of rapid cooling air-cooler have reached a low level, and the evaporator is operating at high energy consumption and low refrigeration capacity. At such a point, it needs to defrost to maintain efficient operation.

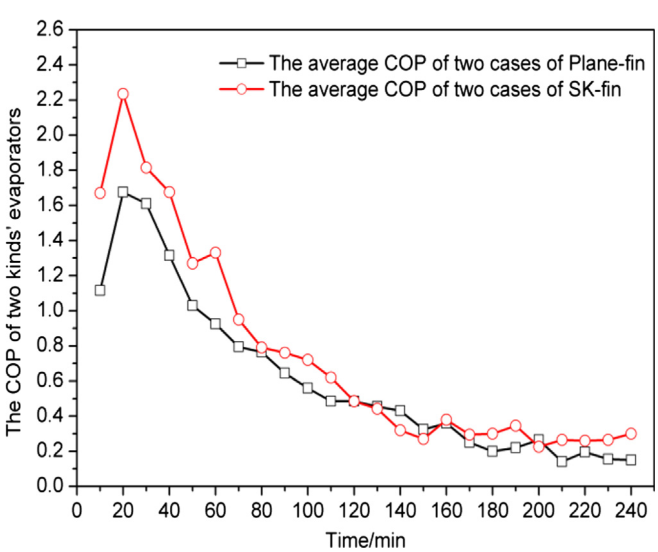

Fig. 7. Variation of *COP* over 4 h running time.

Fig. 7 also illustrates that the *COP* value of SK-type fin prototype is always higher than that of the plane fin prototype during the continuous operation time of 2 h (calculation results shown in Table 4). The average *COP* value of SK-type prototype is 22.65% higher than that of the plane fin prototype within the continuous operation time of 2 h due to several factors: (1) Circular holes in the SK-type fin not only damage the formation of flow boundary layer, but also increase the airflow disturbance, reduce the weak zone area, and improve the efficiency of the fin heat exchanger, all significantly boosting the refrigeration capacity of the SK-type fin; (2) While the plane fin prototype is under frost conditions, the efficiency of its heat exchanger is worse than that of the SK-type fin prototype heat exchanger. In the plane fin heat exchanger, the temperature of the basic tube is lower, the surface of fin frosts faster, and the heat exchanger efficiency continues to deteriorate, all forcing the refrigerant in the tubes of evaporator to be sucked into the compressor without sufficiently gasifying and thus increasing the power consumption of the compressor.

Due to limited finances for this experiment, the prototypes used were made by a professional manufacturer, and the condenser and compressor used were already existing laboratory equipment. This reality, which results in the comparatively low *COP* observed in the experiment, can be explained as "wasting one's talent on a petty job", as using entirely customized, state-of-the-art equipment would give more satisfying results. That said, the use of a comparative experimental study framework, where both types of heat exchangers were tested under the same conditions, should ensure that the validity of the results are not affected. Additionally, the present results are consistent with the earlier wind tunnel experiments [16,19], which fully illustrate the advantages that the SK-type fin offers in terms of superior heat transfer enhancement effects making it a viable alternative to the presently used rectangular refrigeration heat exchanger.

5. Conclusion

In this paper, the refrigerating capacity of a plane fin prototype was compared with that of a new SK-type fin prototype, and the comparison showed that the SK-type fin offers many advantages. During the first 2 h of continuous operation, when the amount of the refrigerant charge are equal and face velocity and ambient conditions are approximately the same, the refrigerating capacity of the SK-type prototype increases by 9.13% on average, while the

Table 4
Comparison of heat exchanger performance at 2 h running time.

Working condition	Fin type	Refrigerating capacity Q_0 (KJ)	Power consumption W (KJ)	COP	$Q_{0,sk}/Q_{0,p}$	W_{sk}/W_p	COP_{sk}/COP_p
Case 1	Plane fin	119286.9	71640	1.67	1.08	0.879	1.225
	SK fin	128535.4	63000	2.04			
Case 2	Plane fin	111267.7	69120	1.61	1.1	0.896	1.228
	SK fin	122423.8	61920	1.98			

power consumption reduces by an average by 11.25% and the *COP* of the compressor increases by 22.65%. Moreover, in the first hour of continuous operation, the energy conservation advantage of the SK-type prototype is even more remarkable. Within 4 h, the refrigeration capacity and energy efficiency of the SK-type prototype are higher than those of the plane fin prototype. The energy performance of the SK-type prototype is most significant during the first 2 h of the experiment, and over the new 2 h of running time, the energy conservation advantage of the SK-type prototype gradually reduces. However, in tandem with this decrease, the SK-type prototype still maintains its characteristic enhancement of heat transfer under frost conditions in 4 h. But in this experimental study, the results suggest that the defrosting time interval should not exceed 2 h, otherwise the energy consumption will be dramatically reduced. When the running time of the prototype exceeded 2 h, the fin surface becomes completely covered by the frosting layer, which leads to the *COP* of both prototypes is lower than 0.6. At this time the heat exchanger efficiency is very poor.

Acknowledgements

The authors are grateful for the supports of Research and Engineering Demonstration of Green Retrofitting Technologies for Office Building (Project No. 2012BAJ06B05), the 111 Project (No.B13041) and the National Key Technologies R&D Program (Project No.2011BAJ03B13). We also wish to thank Dr. Adamson Lyson Thengolose for his assistance in checking the study's English.

References

[1] J.Y. Jun, Investigation of heat transfer characteristics on variation kinds of fin-and-tube heat exchangers with interrupted surfaces, Heat Mass Transfer 42 (1999) 2375–2385.
[2] J.D. Yonko, C.F. Sepsy, An investigation of the thermal conductivity of frost while forming on a flat horizontal plate, ASHRAE Trans. 73 (1967) 2043–2053.
[3] R. Yun, Y. Kim, M. Min, Modeling of frost growth and frost properties with airflow over a flat plate, Int. J. Refrig. 25 (2002) 362–371.
[4] Y.B. Lee, S.T. Ro, An experimental study of frost formation on a horizontal cylinder under cross flow, Int. J. Refrig. 24 (2001) 468–474.
[5] D.K. Yang, K.S. Lee, S. Song, Modeling for predicting frosting behavior of a fin-tube heat exchanger, Int. J. Heat Mass Transfer 49 (2006) 1472–1479.
[6] S.K. Padhmanabhan, D.E. Fisher, L. Cremaschi, E. Moallem, Modeling non-uniform frost growth on a fin-and-tube heat exchanger, Int. J. Refrig. 34 (2011) 2018–2030.
[7] W.M. Yan, H.Y. Li, Y.L. Tsay, Thermofluid characteristics of frosted finned-tube heat exchangers, Int. J. Heat Mass Transfer 48 (2005) 3073–3080.
[8] Y. Kim, Heat transfer characteristics of flat plate finned-tube heat exchangers with large fin pitch, Int. J. Refrig. 28 (2005) 851–858.
[9] J.R. Barbosa Jr., C. Melo, C.J.L. Hermes, P.J. Waltrich, A study of the air-side heat transfer and pressure drop characteristics of tube-fin 'no-frost' evaporators, Appl. Energy 86 (2009) 1484–1491.
[10] J.R. Barbosa Jr., C.J.L. Hermes, C. Melo, CFD analysis of 'no frost' evaporators, J. Braz. Soc. Mech. Sci. Eng. 22 (2010) 445–453.
[11] P.J. Waltrich, J.R. Barbosa Jr., J.L. Christian, B. Hermes, C. Melo, Air-side heat transfer and pressure drop characteristics of accelerated flow evaporators, Int. J. Refrig. 34 (2011) 484–497.
[12] H.H. Wang, S.M. Tan, C. Jiang, Experimental research on heat transfer and resistance of the rectangular fin with changed geometry, J. Chongqing Jianzhu Univ. 4 (1999) 35–39.
[13] S. Hua, Experimental Study on Heat Transfer and Flow Resistance Performance of Turbulent Hole Fins-tubes and Numerical Analysis of Fin Efficiency, Master Degree, Chongqing Jianzhu University, Chongqing, P.R. China, 1999.
[14] J.W. Gao, Study on the Heat Transfer and Refrigeration Performance of Fin-tube with Circular Hole under the Frost Condition and General Program of Rectangular Plane Fin Efficiency, Master Degree, Chongqing Jianzhu University, Chongqing, P.R. China, 2005.
[15] H.H. Wang, J.W. Gao, X.W. Peng, Experimental study on refrigeration performance of fin-tube with circular hole under the frost condition, J. Chongqing Jianzhu Univ. 5 (2007) 4–10.
[16] Z.S. Fang, Research on Energy Conservation Performance of Fin-tube Refrigeration Heat Exchanger with Circular Holes, Degree of Master of Chongqing University, Chongqing, 2008.
[17] H.H. Wang, Z.S. Fang, X.L. Bai, Refrigeration Heat Exchanger Using Three Symmetrical Big Circular Holes Fin and Heat Exchanger, 2009. China, 2008201000634.
[18] H.H. Wang, Z.S. Fang, Numerical simulation of flow and heat transfer with airflow over holes in fin-tubes, J. TongJi Univ. 37 (2009) 969–973.
[19] H.H. Wang, Z.S. Fang, S.Y. Zheng, Experimental investigation on energy conservation performance of fin-tube refrigeration heat exchanger with circular holes, J. Southwest Jiao Tong Univ. 44 (2009) 455–460.
[20] K. Kim, D.R. Kim, K.S. Lee, Local frosting behavior of a plated-fin and tube heat exchanger according to the refrigerant flow direction and surface treatment, Int. J. Heat Mass Transfer 64 (2013) 751–758.